Mechanistic insights into ethidium bromide removal by palygorskite from contaminated water

Po-Hsiang Chang[a,*], Binoy Sarkar[b,*]

[a] *School of Human Settlements and Civil Engineering, Xi'an Jiaotong University, 28 Xianning West Road, Xi'an, Shaanxi, 710049, P.R. China*

[b] *Lancaster Environment Centre, Lancaster University, Lancaster, LA1 4YQ, United Kingdom*

[*] Corresponding author. Email: tectonicion@xjtu.edu.cn (P.-H. Chang); b.sarkar@lancaster.ac.uk (B. Sarkar)

Highlights

- PFl-1 palygorskite was used for ethidium bromide (EtBr) removal from water.
- EtBr removal was as high as 275 mmol/kg corresponding to 108 mg/g.
- Cation exchange was the main adsorption mechanism.
- EtBr dimerization facilitated adsorption at high adsorbate concentration.
- Kinetic equilibrium reached in 1 h; followed pseudo-second order model.

Abstract

Ethidium bromide (EtBr)-containing wastewater can be hazardous to biodiversity when released into the soil and water bodies without treatment. EtBr can mutate living microbial cells and pose toxicity to even higher organisms. This work investigated the removal of EtBr from aqueous solutions by a naturally occurring palygorskite (PFl-1) clay mineral via systematic batch adsorption experiments under different physicochemical conditions. EtBr existed in an undissociated form at pH ~ 7, and was adsorbed on PFl-1 obeying the Freundlich isotherm model. The maximum EtBr adsorption capacity was 285 mmol/kg. The best fitted kinetic model for EtBr adsorption was the pseudo-second order model. The amounts of exchangeable cations desorbed from PFl-1 during EtBr adsorption was linearly correlated to the amounts of EtBr adsorbed, with a slope of 0.97, implying that a cation exchange-based adsorption mechanism was dominating. Additionally, dimerization of EtBr molecules via bromide release assisted an increased EtBr removal by PFl-1 at high adsorbate concentrations. Detailed x-ray diffraction, Fourier transform infrared, scanning electron imaging and energy dispersive x-ray analyses confirmed that EtBr adsorption occurred dominantly on the surface of palygorskite which mineralogically constituted 80% of the bulk PFl-1 adsorbent. A small portion of EtBr was also adsorbed by PFl-1 through intercalation on the smectite impurity (10%) in PFl-1. This study suggested that PFl-1 could be an excellent natural material for removing EtBr from

pharmaceutical and laboratory wastewater.

Keywords: Adsorption; Cation exchange; Contaminants removal; Ethidium bromide; Palygorskite; Pharmaceutical wastewater.

1. Introduction

Ethidium bromide (EtBr, 3,8-diamino-6-phenyl-5-ethylphenanthridine bromide) is an aromatic compound, and had a tricyclic structure with aniline on either side of a pyridine moiety (Fig. S1a). EtBr is the most commonly used nucleic acid fluorescent dye for single cell gel electrophoresis (SCGE), which is a micro-assay technology with high diagnostic value for DNA damage of mononuclear cells (Ge et al., 2014, Singer et al., 1999, Thititananukiji et a., 2010, Waring, 1975). However, EtBr has high toxicity and carcinogenicity to human cells (Singer et al., 1999, Thititananukiji et al., 2010, Waring, 1975). It is also considered to be a teratogen, and a positive chemical mutagen (Armand et al., 2004). Contamination of drinking water with EtBr has become a slowly emerging problem in the water environment, especially in urban areas (Dobaradran et al., 2010, Kikuchi, 2001, Nakano et al., 2000). Taken on a global scale, the widespread practice of SCGE assay may cause a lot of untreated EtBr leaving from research laboratories each year. Therefore, there is a certain hazard to the operator and the laboratory

54 environment from EtBr, and harmless treatment of the compound is an important task in the
55 laboratory. Additionally, if EtBr-containing wastewater is deliberately or accidentally released
56 into the soil or water bodies, that may cause a tremendous hazard to biodiversity because EtBr
57 can mutate living microbial cells and pose toxicity to higher organisms (Li et al., 2020). Removal
58 of EtBr from laboratory wastewater is therefore a matter of immense importance.
59 The use of clay minerals for removing contaminants from wastewater has been extensively
60 studied for decades. Easy availability across continents, minimal pretreatment needed for use,
61 and inexpensiveness of clay minerals give them an edge over other materials in contaminants
62 removal applications (Sarkar et al., 2019; Yuan et al., 2013). Depending on the type, composition
63 and modification of clay minerals, they remove contaminants from water by adsorption, catalytic
64 degradation, or redox-transformation (Zhu et al., 2016). Among the above removal methods,
65 adsorption has been found as the most popular one because of its easy operational requirements,
66 and relatively higher contaminant removal efficiency compared to other methods without much
67 investment for complex modification of the adsorbent or requirement for additional chemicals
68 (Chang et al., 2012, 2014, 2016; Li et al., 2020).
69 Although clay minerals have been applied for removing numerous organic and inorganic
70 contaminants in aqueous media, reports on their use for the adsorptive removal of EtBr from
71 water has been limited in the literature. EtBr adsorption by swelling and mixed-layer clay

mineral such as rectorite was recently studied (Li et al., 2020), and the results showed that EtBr could be intercalated in the interlayers of rectorite. Additionally, bromide ions present in EtBr molecules played a significant role in the formation of dimers which enhanced the EtBr adsorption capacity of the clay mineral (Li et al., 2020). The authors reported that the maximum EtBr adsorption capacity by rectorite was 400 mmol/kg corresponding to 160 mg/g at pH 4.6, and the ratio of solid/solution was 0.2 g/20 mL (Li et al., 2020). The study by Li et al. (2020) showed encouraging results for using natural clay minerals to remove EtBr contaminants from wastewater, and suggested further investigations to test other commonly occurring swelling and non-swelling type clay minerals for this purpose. The key mechanistic difference between swelling and non-swelling clay minerals to remove EtBr ought to be the lack of EtBr intercalation within the interlayers of non-swelling clay minerals (Chang et al., 2009). Nevertheless, both swelling and non-swelling clay minerals in their natural form would have negative surface charges which might also participate in EtBr adsorption via electrostatic interaction with the ethidium (Et^+) cations. However, due to paucity of reported studies, the mechanisms of EtBr adsorption by natural clay minerals are still least understood.

Palygorskite is a non-swelling clay mineral which has been less explored for environmental applications in comparison to swelling type clay minerals such as montmorillonite and rectorite. Palygorskite is a 2:1 type (two tetrahedral sheets and one octahedral sheet) clay mineral with a

unique fibrous structure. Due to its non-swelling nature, palygorskite ought to have better permeability under flow conditions than swelling type clay minerals, and this property might give an edge to the application of palygorskite for EtBr removal in a column set up (Sarkar et al., 2010; Sarkar et al., 2012; Sarkar and Naidu, 2015). It could be hypothesised that unlike rectorite (Li et al., 2020), palygorskite would adsorb EtBr on the outer surface through electrostatic attraction and EtBr dimer formation but not via intercalation in the interlayers. Compared to rectorite, the palygorskite adsorption system would have a different influence of the clay morphology and unique relationship between the clay-desorbed cations and adsorbed EtBr molecules, which were never studied earlier. Therefore, the current study aims to: (1) explore the adsorptive removal of EtBr by a palygorskite clay mineral (PFl-1) in aqueous media via investigating the adsorption isotherm, kinetics, thermodynamics, and effects of pH on adsorption, and (2) deduce the plausible mechanisms of EtBr adsorption by palygorskite through adsorption modelling and extensive adsorbent characterization studies. To the best of the authors' knowledge, there was no previous study reporting EtBr adsorption by palygorskite clay mineral. Therefore, this study has the potential to come up with a new inexpensive adsorbent for efficient removal of EtBr from wastewater.

2. Materials and methods

2.1 Materials

Ethidium bromide (EtBr, $C_{21}H_{20}BrN_3$, CAS No. 1239-45-8) has a molecular weight of 394.294 (Fig. S1a). The aqueous solubility of EtBr is 40 g/L. Different forms of EtBr can be found at pKa values 0.71 and 2.43 at 20 ºC (Fig. S1b) (Zimmermann and Zimmermann, 1976). The molecular size of EtBr is 10.0 x 11.0 x 0.5 Å derived from the calculation using ChemSketch software. The palygorskite (PFl-1) was obtained from the Clay Minerals Society (Chantilly, VA, USA), and was used in this study without any purification. The chemical composition (%) of PFl-1 was: SiO_2: 60.9, Al_2O_3: 10.4, TiO_2: 0.49, Fe_2O_3: 2.98, FeO: 0.40, MnO: 0.058, MgO: 10.2, CaO: 1.98, Na_2O: 0.058, K_2O: 0.80, F:0.542, P_2O_5: 0.80, S: 0.11 (http://www.clays.org/sourceclays_data.html). It contained 80% palygorskite, 10% smectite, 7% quartz, 2% feldspar, and 1% other minerals (Chipera and Bish, 2001). The reported cation exchange capacity (CEC) and specific surface area (SSA) values of PFl-1 were 195 meq/kg and 136.35 m^2/g, respectively, with Ca as the major exchangeable cation (http://www.clays.org/sourceclays_data.html).

2.2 Batch EtBr adsorption experiments

To each 50 mL centrifuge tube, 0.2 g of PFl-1 and 20 mL of EtBr solution were added. All tubes were wrapped with aluminum foils to prevent light-induced decomposition of the compound. For

all experiments, except the isotherm study, the initial EtBr concentration was 4 mmol/L. Previous studies reported that the isothermal EtBr adsorption curve reached the plateau at around 4 mmol/L concentration (Chang et al., 2014; Donğan et al., 2009; Li et al., 2020). The initial pH of EtBr solution was 8.12. After adsorption tests without any pH adjustment, the final solution pHs were almost close to 8 (pH~ 7.9 to 8.18), which were higher than the pK_{a2} value of EtBr, except in the pH dependent adsorption study. For the kinetic study, the mixing time was 0.016, 0.033, 0.083, 0.25, 0.5, 1.0, 2.0, 4.0, 8.0, 16.0 and 24.0 h. For pH adsorption edge experiment, the equilibrium solution pH was varied between 2 and 11 adjusted by adding 2M NaOH or 2M HCl drop-wise, and pH was checked periodically. The purpose of using high concentration of NaOH or HCl was to minimize the change in total liquid volume. For ionic strength experiment, NaCl and $CaCl_2$ were used as the ionic strength adjustor with concentrations of 0.001 M, 0.01 M, 0.1 M, and 1.0 M. For temperature dependent adsorption test, the temperature was maintained at 303, 318, and 333 K. For the isotherm study, the initial EtBr concentrations were 1, 2, 3, 4, 5, 6, 7, and 8 mmol/L. The mixtures were shaken on a reciprocal shaker at 150 rpm for 24 h for all experiments other than the kinetic study. After equilibration, the mixtures were centrifuged at 5000 rpm for 5 min, and the supernatants were passed through 0.22 μm nylon filters before being analyzed by an UV-Vis spectrometer (EtBr concentration) and ion chromatography (metal cation concentration). All adsorption experiments were run in duplicate.

144

145 *2.3 Methods of analyses*

146 EtBr was quantified by an DR5000 UV-Vis spectrophotometer (Hach, Loveland, USA). A UV
147 detector at the wavelength of 480 nm was used (Carbajo et al., 2011). The standards were
148 adjusted to the same pH as the sample supernatants. Calibration curve was made with five
149 standard EtBr concentrations between 0.01 and 0.2 mmol/L with r^2 value no less than 0.998.
150 The metal cations desorbed from PFl-1 during the adsorption of EtBr were analyzed by an
151 Integrion™ high-pressure ion chromatography (HPIC) system (Dionex, Thermo Fisher
152 Scientific™, Waltham, USA) equipped with a Dionex IonPac^{TM} CS12A-5µm column (3 x 150
153 mm). A mobile phase made of 1.922 mL of 20 mM methanesulfonic acid in 1L of water was
154 used. At a flow rate of 0.5 mL/min, the retention time for Na^+, K^+, Mg^{2+}, and Ca^{2+} was 2.7, 3.78,
155 5.92, and 7.38 min, respectively. The bromide (Br^-) anion in the EtBr adsorption media was
156 analyzed by the same HPIC system using a Dionex IonPac^{TM} AS22-Fast-4µm column (2 × 150
157 mm), and a mobile phase made of 4.5 mM Na_2CO_3 in 1L of water. At a flow rate of 0.5 mL/min,
158 the retention time for Br^- was 2.2 min.

159

160 2.4 Characterization of palygorskite

161 Powder X-ray diffraction (XRD) patterns of samples were recorded on a Bruker D8 Advance

A25 Diffractometer (Bruker, Hamburg, Germany) equipped with the LYNXEYE XE detector, using Cu Kα1 radiation in the 2°-10° 2θ range, and a counting time of 0.01 s/step.

The field emission scanning electron microscope (FE-SEM) observation was made on a TESCAN MAIA3 instrument (TESCAN, Brno, Czech Republic) using an acceleration voltage of 15 kV. Energy-dispersive X-ray spectroscopy (EDS) analysis was conducted using X-Max^N Silicon Drift detector (Oxford Instruments NanoAnalysis, High Wycombe, UK) attached to the SEM. Platinum (Pt)-coated samples (~10 nm) was prepared before the SEM observation.

Thermogravimetric (TG) analyses were performed on a NETZSCH STA 449 F5 Jupiter instrument (Netzsch, Deutschland, Germany) with a heating rate of 10 °C/min under N_2 condition. The initial sample weight was between 5 and 10 mg.

Fourier transform infrared (FTIR) spectra were acquired on a Nicolet iS10 spectrometer (Thermo Fisher Scientific™, Waltham, USA) using KBr pressing method. The spectra were obtained in the wavelength range of 4000 – 400 cm^{-1} by accumulating 256 scans at a resolution of 4 cm^{-1}.

3. Results and discussion

3.1 Kinetic adsorption

Many studies about the adsorption of contaminants on clay minerals showed that the adsorption equilibrium was reached almost always in less than 24 h interaction time (Chang et al., 2009,

Donğan et al., 2004, Figueroa et al., 2004, Li et al., 2011a, b). Based upon those previous reports, kinetic experiment was conducted up to 24 h in this study. However, the adsorption of EtBr on PFl-1 reached equilibrium in about only 1 h (Fig. S2). The pseudo-second-order kinetic model yielded the best fitting with a high coefficient of determination ($R^2 > 0.999$). The integrated rate law for the pseudo-second-order model is (Eq. 1) (Ho and McKay, 1999):

$$q_t = \frac{kq_e^2 t}{1 + kq_e t} \qquad \text{(Eq. 1)}$$

where, k (kg/mmol.h) is the rate constant of adsorption, q_e (mmol/kg) is the amount of EtBr adsorbed at equilibrium, and q_t (mmol/kg) is the amount of EtBr adsorbed on the adsorbent surface at any time, t. Eq. 1 is based on the adsorption capacity which is proportional to the number of active sites occupied on the adsorbent, and can be re-arranged into a linear form (Eq. 2):

$$\frac{t}{q_t} = \frac{1}{kq_e^2} + \frac{1}{q_e} t \qquad \text{(Eq. 2)}$$

where, kq_e^2 is the initial rate (mmol/g.h). For EtBr adsorption, the initial rate was 7143 mmol kg^{-1} h^{-1}, the rate constant was 0.1415 kg $mmol^{-1}$ h^{-1}, and the q_e was 225 mmol/kg, when the adsorption data were fitted to Eq. (2) (Fig. S2). The q_e value agreed with the calculated value of 215 mmol/kg (Fig. S2) obtained from the adsorption isotherm of EtBr. By virtue of the exchange or sharing of electrons between the adsorbent and adsorbate, the pseudo-second-order kinetic model describes chemical sorption as the rate-limiting step which may also involve valence

198 forces (Ho and McKay, 1999, Park et al., 2013). The equilibrium time was 8 min for EtBr
199 adsorption on CuO nanoparticles at an initial concentration of 0.3 mg/L, final pH 9, and
200 adsorbent dose 0.03 g/20 mL (Fakhri, 2014). Besides, the equilibrium time was 3 h for EtBr
201 adsorption on both natural pumice and aluminium-coated pumice at initial concentrations of 30
202 and 100 mg/L, initial pH 8, and adsorbent dose 8 g/L (Heibati et al., 2016). For PFl-1, the EtBr
203 adsorption reached to 88% of its maximum capacity within just 15 min, which indicated that
204 the clay mineral had advantage over other adsorbents in terms of quick removal of EtBr from
205 aqueous solutions.
206
207 *3.2 Equilibrium adsorption*
208 The EtBr adsorption data were fitted using the Langmuir and Freundlich isotherm models (Fig.
209 1). The Langmuir model is described as (Eq. 3):
210 $$C_S = \frac{K_L S_m C_L}{1 + K_L C_L} \quad \text{(Eq. 3)}$$
211 where, C_S is the amount of adsorbate adsorbed on solid phase at equilibrium (mmol/kg), C_L is the
212 equilibrium solute concentration (mmol/L), S_m is the apparent adsorption capacity or adsorption
213 maximum (mmol/kg), and K_L is the Langmuir coefficient (L/mg). Eq. (3) can be rearranged to a
214 linear form Eq. 4 so that K_L and S_m can be determined by a linear regression.

$$\frac{C_L}{C_S} = \frac{1}{K_L S_m} + \frac{C_L}{S_m} \quad \text{(Eq. 4)}$$

The Freundlich adsorption equation can be written as (Eq. 5):

$$C_s = K_F C_L^{1/n} \quad \text{(Eq. 5)}$$

where, K_F is the Freundlich adsorption constant, and n is the Freundlich exponent. A non-linear regression fitting of the isotherm models was conducted using the least squares method (Mukhopadhyay et al., 2019). As for EtBr, the Freundlich model seemed to have the best fitting with a R^2 value of 0. 935, compared to R^2 = 0. 587 for the Langmuir model (Fig. 1). The maximum EtBr adsorption capacity calculated from the Langmuir model was 275 mmol/kg, which was well above 149 mmol/kg (58.82 mg/g) and 195 mmol/kg (76.92 mg/g) for EtBr adsorbed on a natural pumice, and aluminium-coated pumice, respectively, at pH=8 (Heibati et al., 2016). Fitting of the adsorption isotherm data to the Freundlich model suggested that EtBr adsorption on PFl-1 followed a multi-layer adsorption pattern on heterogeneous adsorption sites (Figueroa et al, 2004; Heibati et al., 2016).

3.3 Desorbed cations

The amount of Ca^{2+} desorbed from PFl-1 showed a positive correlation (R^2=0.88) with the amount of EtBr adsorbed at the first two initial EtBr concentrations of 1 and 2 mmol/L (Fig. 2).

232 The amounts of K^+ and Na^+ released from the clay mineral were lower than Ca^{2+}, and almost
233 invariable with respect to the amount of EtBr adsorbed. The amount of Mg^{2+} released was also
234 slightly correlated (R^2=0.99) with the amount of EtBr adsorbed, which was likely because of the
235 higher MgO content in the bulk adsorbent. The results corresponded to the trend of
236 chlorpheniramine (Li et al., 2011a), diphenhydramine (Li et al., 2011b) and amitriptyline (Tsai et
237 al., 2016) adsorption on PFl-1, and further suggested that Mg^{2+} was present in the interlayers of
238 the clay mineral. The ratio of the total desorbed cations to adsorbed amounts of EtBr was 0.97
239 (Fig. 2) at initial EtBr concentration < 2 mmol/L, which indicated that cation exchange was the
240 main mechanism for EtBr adsorption on PFl-1 at those adsorbate concentrations. In terms of
241 adsorption capacity, the maximum adsorption capacity was 160 mmol/kg below the initial EtBr
242 concentration of 2 mmol/L, and accompanied by cation desorption (Fig. 2). However, the cation
243 desorption from the clay mineral was decreased above the initial EtBr concentration of 2
244 mmol/L, while the EtBr adsorption still was continuing, implying that a second mechanism was
245 also involved to improve the EtBr adsorption capacity at high initial adsorbate concentrations.
246
247 *3.4 Effect of solution pH and competing cation on EtBr adsorption*
248 The point of zero charge (PZC) of many adsorbents significantly influence their contaminant
249 adsorption capacities when electrostatic attraction is the key mechanism of reaction (Castaldo et

al., 2019; Vasudevan et al., 2009). The pH_{pzc} of PFl-1 was reported to be 4.1 (Panagiota et al., 2007). The EtBr adsorption capacities on PFl-1 at various pH values are shown in Fig. S3a. The descending trend of adsorption capacity with decreasing pH values indicated that pH_{pzc} was an influencing factor for EtBr adsorption on PFl-1, which was different from results reported in previous studies where the adsorption capacities were unchanged between pH 2 to 11 (Chang et al., 2014, Wang et al., 2010). The positive charge of PFl-1 below pH 4.1 seemed to repulse the positively charged Et^+ ions, and abruptly reduce the EtBr adsorption capacity from 200 mmol/L (at pH = 5) to 133 mmol/L (at pH < 4.1), accounting about 33% drop in adsorption capacity (Fig. S3a). This 33% decline of adsorption capacity at low pH could also be caused by the abundance of H^+ which was added drop-wise through 2M HCl during adjusting pH value of the system. The excess H^+ likely provided a competition to Et^+ for adsorption sites at low pH. However, it was not possible to determine the respective contributions of PFl-1 surface charge alternation and solution H^+ competition toward the ultimate decline of EtBr adsorption at low pH values. On the other hand, the increased negative charge of PFl-1 at high pH values attracted the positively charged Et^+, and increased the adsorption capacity from 200 to 240 mmol/L at pH 5 to 11. Thus, pH_{pzc} of PFl-1 and solution H^+ competition both played significant roles in controlling EtBr adsorption ability of the clay mineral below pH 4.1 and above pH 9 (Fig. S3a).

The CEC of PFl-1 also was a key factor for EtBr adsorption on the clay mineral (Fig. S3b).

Addition of a second cation in the system was expected to decrease the EtBr adsorption through competition effect. However, the competition was not obvious with an increase in concentrations of Na^+ and Ca^{2+} (Fig. S3b). At the lowest concentration of NaCl and $CaCl_2$ (0.001 M), the adsorption capacity of EtBr was 230 mmol/kg, which observed a decrease by only 17% (190 mmol/kg) with the addition of cations (Fig. S3b). These results showed that in addition to the cation exchange mechanism, there was a high affinity between PFl-1 and EtBr in the aqueous system, possibly originating from the Br^- in EtBr (explained later in the paper).

3.5 Effect of temperature on EtBr adsorption

EtBr adsorption capacities decreased with increasing temperature at an initial EtBr concentration of 4 mmol/kg at neutral pH condition (Fig. S4), suggesting an exothermic adsorption process. The thermodynamic parameters of EtBr adsorption on PFl-1 were inferred from the partitioning coefficient values using (Eq. 5):

$$\ln K_d = -\frac{\Delta H}{RT} + \frac{\Delta S}{R} \quad \text{(Eq. 5)}$$

where, T is the temperature in K, R is the gas constant (8.314 J/mol•K), ΔH is the change in enthalpy, and ΔS is the change in entropy after adsorption. The free energy of adsorption ΔG is linked to these thermodynamic parameters by (Eq. 6):

$$\Delta G = \Delta H - T\Delta S \quad \text{(Eq. 6)}$$

Negative ΔG values obtained in this study (Table 1) suggested a spontaneous adsorption process, and also indicated the high affinity between PFl-1 and EtBr during the adsorption process (Eldaroti et al., 2013, Li et al., 2020, Moradi et al., 2013, Zhu et al., 2016). The negative ΔH values (Table 1) indicated an exothermic adsorption process, which was different from an endothermic reaction for EtBr adsorption on carbon nanotubes (Moradi et al., 2013), but agreed with the result of its adsorption on rectorite (Li et al., 2020). Besides, the order or disorder of molecular morphologies depended on the parameter ΔS; the small positive ΔS value (Table 1) indicated that the adsorption was spontaneous by virtue of an increase in the system randomness, as EtBr molecules interacted with the PFl-1 surface.

3.6 XRD analysis

Non-expandable clay minerals such as illite or palygorskite are not expected to exhibit any swelling phenomenon after adsorption of organic molecules (Wick et al., 2018, Youcef et al., 2019). As a result, the strongest reflection position at $2\theta = 8.4°$, corresponding to $d_{110} = 10.53$ Å of palygorskite, in the XRD pattern of PFl-1 did not change after EtBr adsorption (Fig. 3). These results indicated that the adsorption of EtBr occurred on the external surface of palygorskite which was the most abundant (80%) clay mineral in the PFl-1 sample (Fig. 3a, b). However, the palygorskite sample (PFl-1) used in this study contained about 10% smectite (a swelling type

clay) as an impurity (Chipera and Bish, 2001). The smectite thus provided its d_{001} reflection at 15 Å in the XRD pattern of PFl-1 (Chipera and Bish, 2001). No analysis was conducted in this study to confirm the exact type of smectitic clay mineral present in the PFl-1 sample. However, from the observed d_{001} reflection (15 Å), and Mg^{2+} and Ca^{2+} being the major exchangeable cations in the sample (Tsai et al., 2016), a Ca-montmorillonite similar to the source clay SAz-2 (d_{001} = 15.2 Å; Li et al., 2010) could be present. Inevitably, the smectite also participated in EtBr adsorption. As a result, the d_{001} reflection of smectite at 15.0 Å shifted to 17.7 Å, and finally to 18.4 Å after EtBr adsorption at different concentrations and times (Fig. 3a, b). The change of d-values was attributed to the 10% content of smectite in the bulk PFl-1 sample instead of the palygorskite itself. The d-value stopped changing at 0.25 h (Fig. 3b) indicating that the interlayers of smectitic clay mineral were full of EtBr due to the less content of smectite in the bulk adsorbent, and from this point onward the adsorption happened only on the external surface of palygorskite. In other words, most of the EtBr adsorption occurred on the external surface of palygorskite.

3.7 Derivative thermogravimetric (DTG) analyses

The decomposition temperature (T_{peak}) of raw EtBr was 355°C with a mass loss of 57% continuing up to 600°C (Fig. 4a). The DTG curve of PFl-1 showed three T_{peak} values at 70, 210,

and 430°C (Fig. 4b) which corresponded to two steps of dehydration and dehydroxylation temperatures, respectively (Frost and Ding, 2003). Guggenheim and Gross (2001) observed T_{peak} of palygorskite at 83, 220, and 420°C due to dehydration and dehydroxylation of the clay mineral. The T_{peak} of intercalated EtBr on rectorite was observed at 420°C in a previous study (Li et al., 2020). Therefore, it was possible that the T_{peak} of intercalated EtBr on the smectite component (10%) of PFl-1 still happened, but was blinded by the T_{peak} of the palygorskite dehydroxylation at around same temperature (Fig. 4b). This argument was partially supported by the fact that the T_{peak} was slightly uplifted to 440°C with increased EtBr adsorption capacity of PFl-1 (Fig. 4b).

3.8 SEM and EDS analyses

In order to confirm the T_{peak} of clay-intercalated EtBr, and understand the fate of Br^- during EtBr adsorption, SEM (Fig. 5a-f), EDS (Fig. 5g) and further XRD (Fig. 5h-j) investigations were carried out (Fig. 5). The Br^- ions (denoted by Br in EDS) were spread out everywhere on the surface of PFl-1 after adsorption (Fig. 5d), which implied the co-adsorption of Br^- and Et^+ on the adsorbent. After heating the EtBr-loaded sample at 500°C for 2 h (Fig. 5e), the Br^- distribution had not disappeared (Fig. 5f, g). Following the heat treatment, the d-value of smectite (d_{001}) and palygorskite (d_{110}) in PFl-1 was maintained at 13.5 Å and 9.7 Å, respectively (Fig. 5j). The

decomposition of intercalated EtBr located in the interlayers of smectite in PFl-1 rendered the d-value to gradually decrease from 18.4 to 13.5 Å (Fig. 5h-j). These results confirmed that Br^- still existed after heating the EtBr-loaded sample at 500°C for 2 h, and the T_{peak} of smectite-intercalated EtBr was 440°C for PFl-1 although it was blinded by the peak of palygorskite dehydroxylation at around 430°C (Fig. 4b).

3.9 FTIR analyses

The chemical environment of the adsorption complexes on PFl-1 surfaces was examined by IR spectroscopy on the basis of the absorption band properties of individual samples (Fig. 6). The characteristic bands of EtBr should occur at 3302 and 3192 cm^{-1} assigning to $-NH_2$ asymmetric and symmetric stretching vibrations, respectively (Swaminathan et al., 2009). These two bands were not displayed after adsorption of EtBr on PFl-1 (Fig. 6a). It was likely that the $-NH_2$ bands were overlapped by the board bands of PFl-1, and thus did not clearly prove the participation of NH_2 groups in EtBr adsorption (Eldaroti et al., 2013). The disappearance of ν(NH), $\nu_{deformation}(NH_3^+)$, $\delta_{symmetrical}(NH_3^+)$ and $\rho(NH_3^+)$ bands at about 3200, 1600, 1300 and 800 cm^{-1} (Fig. 6b) could also be due to the overlapping of PFl-1 and EtBr bands. Therefore, the above bands did not also confirm the possible protonation of $-NH_2$ groups of EtBr donor via a proton-transfer reaction (from the acidic center of each acceptor to form NH_4^+ based on acid–base

theory) (Adam, 2012, Adam et al., 2012, Bellamy, 1975, Bharathikannan et al., 2008, Gaballa et al., 2012). However, the band position of raw EtBr at 1318 cm^{-1}, which was attributed to Ph-N-$(CH_3)_2$ stretching vibration (Sali et al., 2015), remained intact and did not significantly shift after EtBr adsorption on PFl-1. Other band assignments such as 1499, 1463, 1408, 1352, 1319, and 1262 cm^{-1} were related to ν(C=N), ν(C=C), ν(C-H), ν_{as}(C-N), ν_s(C-N), and δ(C-H), respectively, and all of them also did not shift in the spectra of EtBr-loaded PFl-1 (Fig. 6b). The FTIR investigation thus suggested that only C-H groups participated in the interaction between EtBr and PFl-1 surfaces rather than the -NH_2 groups. However, EtBr adsorption on a swelling type clay mineral rectorite involved the participation of -NH_2 groups as the main contact site when EtBr existed in its monomer form (Li et al., 2020).

3.10 Adsorption mechanism and the role of bromide on contact model

The molecular size of EtBr is 11.0 Å x 10.0 Å x 0.5 Å, and its maximum occupied area is 110 $Å^2$. At the maximum EtBr adsorption capacity of 275 mmol/kg, and with a SSA of 136.35 m^2/g for PFl-1, the occupied area of each EtBr molecule was calculated to be 83 $Å^2$, which was less than the ideal 110 $Å^2$ area of the molecule. Therefore, the SSA of PFl-1 was not enough to inhabit all the EtBr molecules in parallel direction at the maximum EtBr adsorption capacity. One possible model could be the vertical contact, which would touch on the PFl-1 surface with

one side of the EtBr molecules. However, the results from FTIR study showed that the NH_2 groups did not serve as the contact sites, as should be happening in case of the postulated vertical contact model. As a result, the only feasible contact model was that the EtBr molecules were laying on the PFl-1 surface in parallel direction via dimer formation at high EtBr adsorption capacities (Fig. 7). The concept was supported by the fitting of the adsorption data to the Freundlich isotherm model which indicated multi-layer adsorption (Fig. 1). On the other hand, the occupied area per EtBr molecule would be 228, 148, and 123 $Å^2$ corresponding to 0.51, 0.78, and 0.94 CEC coverage of EtBr on PFl-1, respectively. These occupied areas on the PFl-1 surface were enough to contain the maximum size of EtBr molecules in a free style (Fig. 7). The maximum adsorption capacity was 0.8 and 0.96 CEC of PFl-1 at the initial concentration of 2 and 3 mmol/L, respectively. The slope of the desorbed cations vs adsorbed EtBr line was 0.97 (Fig. 2a), suggesting that 97% of cations were desorbed from the PFl-1 surface below the 0.8 CEC equivalent EtBr concentration (Fig. 2a), which indicated that cation exchange was the main adsorption mechanism at that adsorbate concentration. Interestingly, the desorption of cations ceased at EtBr concentrations of 0.8 to 1.40 CEC equivalent of PFl-1 (Fig. 2a), while the adsorption of EtBr still continued. As a result, the adsorption seemed to involve a second mechanism to boost up the adsorption capacity above the 0.96 CEC equivalent EtBr concentration. The FTIR results suggested that there was no hydrogen bonding between the

394 adsorbent and adsorbate. The hydrophobicity might be one possible interaction, but there was no
395 evidence of such phenomenon in this study. In order to unearth the contributory mechanism, the
396 analysis of Br^- concentration in the adsorption system was therefore undertaken. The adsorption
397 reached equilibrium at the initial EtBr concentration of 8 to 14 mmol/L (Fig. 1), meanwhile, the
398 desorption of cations was stopped during adsorption from these four adsorbate concentrations
399 (Fig. 2a). However, the adsorption of Br^- progressively increased from the initial concentration
400 of 8 to 14 mmol/L (Fig. 2b). The EtBr molecules could form dimers via the parallel orientation
401 of Br^- (Thomas and Roques, 1972), which was supported by the calculation of the electronic
402 structure (occupancy area) of EtBr (Giacomoni and Bret, 1973). The dimer concentration would
403 be 3 mM while the monomer concentration would be 7 mM at the initial EtBr concentration of
404 10 mM, according to the theoretical calculation (Benfield et al., 2011). Besides, the dimer
405 concentration would be calculated as 5.5 mM using the 133 M^{-1} dimerization constant for EtBr at
406 its initial concentration of 10 mM (Veselkov et al., 1994). The residue of Br^- was 4.4 mM in the
407 solution under the initial EtBr concentration of 10 mM (Fig. 2b), leaving 5.6 mM of Br^-
408 adsorbed. Therefore, the monomers and dimers of EtBr should have been co-adsorbed on PFl-1,
409 which was also supported by the results of SEM and EDS. This mechanism agreed with the fact
410 that the adsorption still increased while the cation desorption ceased under initial EtBr
411 concentrations from 8 to 14 mM (Fig. 2a). Consequently, the Br^- played an important role in

EtBr adsorption on the clay mineral by participating in the dimerization reaction, which enhanced the adsorption up to the tune of 1.39 CEC of PFl-1. Consequently, the dimer formation mechanism corroborated with the Freundlich model fitting of the EtBr adsorption data in this study, which was different from the Langmuir model fitting for EtBr adsorption on rectorite (Li et a., 2020).

4. Conclusions

The current study showed that the adsorption of EtBr on PFl-1 happened quickly within 1 h, and with a spectacular adsorption capacity of 275 mmol/kg corresponding to 108 mg/g. The adsorption capacity was greater than the CEC value of the clay mineral. The desorption of inorganic cations agreed with Et^+ adsorption, confirming the main mechanism of EtBr removal occurred through the exchange for Et^+ by Ca^{2+} on PFl-1. Adsorption of counterion Br^- accompanying Et^+ suggested the formation of dimers of Et^+ on the external surface of PFl-1 at higher adsorption capacities. Moreover, the dimer alignment rendered an adsorption capacity enhancement, which was supported by fitting of the adsorption data to the Freundlich isothermal model. Results of this study thus suggested that PFl-1 could be used as a potential natural adsorbent for removing EtBr and similar cationic organic contaminants (e.g., dye compounds) from pharmaceutical and laboratory wastewater. The non-swelling and easy liquid flow

behaviors of PFl-1 could facilitate practical application of this natural material in a fixed-bed wastewater treatment system. Future research is needed to further understand the matrix effects of laboratory and pharmaceutical wastewater on the performance for EtBr removal by PFl-1 in batch and pilot scale studies.

Acknowledgement

This research was financially supported by the Grant No. 1191319102 from Xi'an Jiaotong University, Shaanxi, P.R. China. The authors are thankful to the core facilities sharing platform of Xi'an Jiaotong University for their instruments such as HPIC, XRD, FE-SEM, TGA, and FT-IR used in this research.

Declaration of interest

The authors declare no competing financial interests for this study.

References

Adam, A.A., 2012. Synthesis, spectroscopic, thermal and antimicrobial investigations of charge-transfer complexes formed from the drug procaine hydrochloride with quinol, picric acid and TCNQ. J. Mol. Struct. 1030, 26–39.

Adam, A.A., Refat, M.S., Sharshar, T., Heiba, Z.K., 2012. Synthesis and characterization of highly conductive charge-transfer complexes using positron annihilation spectroscopy. Spectrochim. Acta, Part A 95, 458–477.

Armand, R., Channon, J.Y., Kintner, J., White, K.A., Miselis, K.A., Perez, R.P., Lewis, L.D., 2004. The effect of ethidium bromide induced loss of mitochondrial DNA on mitochondrial phenotype and ultrastructure in a human leukemia T-cell line (MOLT4 cells). Toxicol. Appl. Pharm. 196, 68–79.

Bellamy, L.J., 1975. The Infrared Spectra of Complex Molecules, Chapman & Hall, London.

Benfield, C.T., Mansur, D.S., McCoy, L.E., Ferguson, B.J., Bahar, M.W., Oldring, A.P., Grimes, J.M., Stuart, D.I., Graham, S.C., Smith, G.L., 2011. Mapping the IκB kinase β (IKKβ)-binding interface of the B14 protein, a vaccinia virus inhibitor of IKKβ-mediated activation of nuclear factor κB. J. Biol. Chem. 286, 20727–20735.

Bharathikannan, R., Chandramohan, A., Kandhaswamy, M.A., Chandrasekaran, J., Renganathan,

R., Kandavelu, V., 2008. Synthesis, crystal growth and properties of the charge transfer complex adduct of 2-nitro aniline with picric acid – An organic non-linear optical material. Cryst. Res. Technol. 43, 683–688.

Carbajo, J., Adán, C., Rey, A., Martínez-Arias, A., Bahamonde, A., 2011. Optimization of H_2O_2 use during the photocatalytic degradation of ethidium bromide with TiO_2 and iron-doped TiO_2 catalysts. Appl. Catal. B: Environ. 102, 85–93.

Castaldo, R., Ambrogi, V., Gentile, G., 2019. Composite Nanoadsorbents. Chapter 2-Microporous Organic Polymer Nanocomposites for Adsorption Applications. Composite Nanoadsorbents-Micro and Nano Technologies, p.25–47.

Chang, P.-H., Li, Z. Yu, T.-L., Munkhbayer, S., Kuo, T.-H., Hung, Y.-C., Jean, J.-S., Lin, K.-H., 2009. Sorptive removal of tetracycline from water by palygorskite. J. Hazard. Mater. 165, 48–155.

Chang, P.-H., Li, Z., Jean, J.-S., Jiang, W.-T., Wang, C.-J., Lin, K.-H., 2012. Adsorption of tetracycline on 2:1 layered non-swelling clay mineral illite. Appl. Clay Sci. 67-68, 158–163.

Chang, P.-H., Jiang, W.-T., Li, Z., Kuo, C.-Y., Jean, J.-S., Chen, W.-R., Lv, G., 2014. Mechanism of amitriptyline adsorption on Ca-montmorillonite (SAz-2). J. Hazard. Mater. 277, 44−52.

Chang, P.-H., Jiang, W.-T., Li, Z., Kuo, C.-Y., Wu, Q., Jean, J.-S., Lv, G., 2016. Interaction of ciprofloxacin and probe compounds with palygorskite. J. Hazard. Mater. 303, 55–63.

Chipera, S.J., Bish, D.L., 2001. Baseline studies of the Clay Minerals Society source clays: powder X-ray diffraction analyses. Clays Clay Min. 49, 398–409.

Dobaradaran, S., Nabizadeh, R., Mahvi, A.H., Mesdaghinia, A.R., Naddafi, K., Yunesian, M., Rastkari, N., Nazmara, S., 2010. Survey on degradation rates of trichloroethylene in aqueous solutions by ultrasound. Iran J. Environ. Health Sci. 7, 307–312.

Donğan, M., Alkan, M., Turkyilamz, A., Ozdemir, Y., 2004. Kinetic and mechanism of removal of methylene blue by adsorption onto perlite. J. Hazard. Mater. 109, 141–148.

Fakhri, A., 2014. Assessment of ethidium bromide and ethidium monoazide bromide removal from aqueous matrices by adsorption on cupric oxide nanoparticles. Ecotoxicol. Environ. Saf. 104, 386–392.

Figueroa, R.A., Leonard, A., MacKay, A.A., 2004. Modeling tetracycline antibiotic sorption to clays. Environ. Sci. Technol., 38, 476–483.

Eldaroti, H.H., Gadir, S.A., Refat, M.S., Adam, A.M.A., 2013. Preparation, spectroscopic and thermal characterization of new charge-transfer complexes of ethidium bromide with π-acceptors: In vitro biological activity studies. Spectrochim. Acta, Part A 109, 259–271.

Frost, R.L., Ding, Z., 2003. Controlled rate thermal analysis and differential scanning

calorimetry of sepiolites and palygorskites. Thermochim. Acta 397, 119–128.

Gaballa, A.S., Teleb, S.M., Nourc, E.M., 2012. Preparation and spectroscopic studies on charge-transfer complexes of famciclovir drug with different electron acceptors. J. Mol. Struct. 1024, 32–39.

Ge, J., Prasongtanakij, S., Wood, D.K., Weingeist, D.M., Fessler, J., Navasummrit, P., Ruchirawat, M., Engelward, B.P., 2014. CometChip: a high-throughput 96-well platform for measuring DNA damage in microarrayed human cells. J. Vis. Exp. 92, 50607–50607.

Giacomoni, P.U., Bret, M., 1973. Le electronic structure of ethidium bromide. FEBS Lett. 29, 227–23.

Guggenheim, S., Groos, A.F.K., 2001. Baseline studies of the clay minerals society source clays: thermal analysis. Clay Clay Miner. 49, 433–443.

Heibati, B.K., Yetilmezsoy, K., Zazouli, M.A., Rodriguez-Couto, S., Tyagi, I., Agarwal, S., Gupta, V.K., 2016. Adsorption of ethidium bromide (EtBr) from aqueous solutions by natural pumice and aluminium-coated pumice. J. Mol. Liq. 213, 41–47.

Ho, Y.S., McKay, G., 1999. Pseudo-second order model for sorption processes. Process Biochem. 34, 451–465.

Kikuchi, H., 2001. The investigation about the nature measurement result of 1999 groundwater quality and a groundwater-contamination example. Water Waste, 43, 396.

Li, Z., Chang, P.-H. Jiang, W.-T., Liu, Y.-J., 2020. Enhanced removal of ethidium bromide (EtBr) from aqueous solution using rectorite. J. Hazard. Mater. 384, 121254.

Li, Z. Chang, P.-H., Jean, J.-S., Jiang, W.-T., Hong. H., 2011a. Mechanism of chlorpheniramine adsorption on Ca-montmorillonite. Colloid Surf. A-Physicochem. Eng. Asp. 385, 213−218.

Li, Z., Chang, P.-H., Jean, J.-S., Jiang, W.-T., Wang, C.-J., 2010. Interaction between tetracycline and smectite in aqueous solution. J. Colloid Interface Sci. 341, 311-319.

Li, Z. Chang, P.-H., Jiang, W.-T., Jean, J.-S., Hong, H., Liao, L., 2011b. Removal of diphenhydramine from water by swelling clay minerals. J. Colloid Interface Sci. 360, 227–232.

Moradi, O., Fakhri, A., Adami, S., Adami, S., 2013. Isotherm, thermodynamic, kinetics, and adsorption mechanism studies of Ethidium bromide by single-walled carbon nanotube and carboxylate group functionalized single-walled carbon nanotube. J. Colloid Interface Sci. 395, 224–229.

Mukhopadhyay, R., Manjaiah, K.M., Datta, S.C., Sarkar, B., 2019. Comparison of properties and aquatic arsenic removal potentials of organically modified smectite adsorbents. J. Hazard. Mater. 377, 124-131.

Nakano, Y., Li, Q.H., Nishijima, W., Shoto, E., Okada, M., 2000. Biodegradation of trichloroethylene (tce) adsorbed on granular activated carbon (gac). Water Res, 34, 4139–

4142.

Panagiota, S., Kiriaki, L., Dimitrios, G., Thomas, S.G., Yiannis, D., 2007. Physicochemical study of novel organoclays as heavy metal ion adsorbents for environmental remediation. J. Colloid Interf. Sci. 316, 298–309.

Park, Y., Ayoko, G.A., Horváth, E., Kurdi, R., Kristof, J., Frost, R.L., 2013. Structural characterisation and environmental application of organoclays for the removal of phenolic compounds. J. Colloid Interf. Sci. 393, 319–334.

Refat, M.S., El-Korashy, S.A., El-Deen, I.M., El-Sayed, S.M., 2011. Experimental and spectroscopic studies of charge transfer reaction between sulfasalazine antibiotic drug with different types of acceptors. Drug Test. Anal. 3, 116–131.

Sali, R., Naik, L.R., Bhajantri, R.F., Kamanavalli, C.M., Premakshi, S.G., 2015. Optical and fluorescence study of ethidium bromide doped poly (vinyl alcohol). Int. J. Luminesc. Appl. 5, 131–133.

Sarkar, B., Xi, Y., Megharaj, M., Krishnamurti, G.S.R., Naidu, R., 2010. Synthesis and characterisation of novel organopalygorskites for removal of p-nitrophenol from aqueous solution: Isothermal studies. J. Colloid Interf. Sci. 350, 295–304.

Sarkar, B., Megharaj, M., Xi, Y., Naidu, R., 2012. Surface charge characteristics of organo-palygorskites and adsorption of p-nitrophenol in flow-through reactor system. Chemical

553 Engineer. J. 185–186, 35–43.
554 Sarkar, B., Naidu, R., 2015. Organopalygorskites prepared from quaternary ammonium
555 compounds and their environmental uses. In: Pasbakhsh, P., Churchman, G.J. (Eds.),
556 Natural Mineral Nanotubes: Properties and Applications. Apple Academic Press, pp. 323–
557 340.
558 Sarkar, B., Rusmin, R., Ugochukwu, U.C., Mukhopadhyay, R., Manjaiah, K.M., 2019. Chapter 5
559 - Modified clay minerals for environmental applications, in: Mercurio, M., Sarkar, B.,
560 Langella, A. (Eds.), Modified Clay and Zeolite Nanocomposite Materials. Elsevier, pp.
561 113-127.
562 Singer, V.L., Lawlor, T.E., Yue, S., 1999. Comparison of SYBR Green I nucleic acid gel stain
563 mutagenicity and ethidium bromide mutagenicity in the Salmonella/mammalian
564 microsome reverse mutation assay. Mutat. Res. 439, 37–47.
565 Swaminathan, J., Ramalingam, M., Sethuraman, V., Sundaraganesan, N., Sebastian, S., 2009.
566 Vibrational spectroscopic studies and DFT calculations of 4- aminoantipyrine.
567 Spectrochim. Acta, Part A 73, 593–600.
568 Thititananukiji, S. Vejarafpjmol, R. Pewnjm, T., 2010. Ethidium bromide nuclear staining and
569 fluorescence micmscopy：an alternative method for triploidy detection in fish. J. world.
570 Aquac. Soc. 27, 213–217.

Thomas, G., Roques, B., 1972. Proton magnetic resonance studies of ethidium bromide and its sodium borohydride reduced derivative. FEBS Lett. 26, 169–175.

Tsai, Y.-L., Chang, P.-H., Gao, Z.-Y., Xu, X.-Y., Chen, Y.-S., Wang, Z.-H., Chan, X.-Y., Yang, Z.-Y., Wang, Z.-H., Jean, J.-S., Li, Z., Jiang, W.-T., 2016. Amitriptyline removal using palygorskite clay. Chemosphere 155, 292–299.

Yuan, G.D., Theng, B.K.G., Churchman, G.J., Gates, W.P., 2013. Chapter 5.1 - Clays and Clay Minerals for Pollution Control, in: Bergaya, F., Lagaly, G. (Eds.), Developments in Clay Science. Elsevier, pp. 587-644.

Vasudevan, D., Bruland, G.L., Torrance, B.S., Upchurch, V.G., MacKay, A.A., 2009. pH-dependent ciprofloxacin sorption to soils: Interaction mechanisms and soil factors influencing sorptio. Geoderma 151, 68–76.

Veselkov, A.N., Dymant, L.N., Baranovskiy, S.F., 1994. The study of self-association of ethidium bromide in an aqueous solution by H-NMR spectroscopy. Khim Fizika 13, 72–80.

Wang, C.-J., Li, Z., Jiang, W.-T., Jean, J.-S., Liu, C.-C., 2010. Cation exchange interaction between antibiotic ciprofloxacin and montmorillonite. J. Hazard. Mater. 183, 309–314.

Waring, M., 1975. *in* Antibiotics (Corcoran, J. W., and Hahn, F. E., Eds.), Vol. 3, pp. 141–165, Springer, New York.

Wick, S., Baeyens, B., Fernandes, M. M., Voegelin, A., 2018. Thallium Adsorption onto Illite.

589 Environ. Sci. Technol. 52, 571–580.
590 Youcef, L.D., Belarouia, L.S., López-Galindo, A., 2019. Adsorption of a cationic methylene blue
591 dye on an Algerian palygorskite. Appl. Clay Sci. 179, 105145.
592 Zimmermann, Z. Zimmermann, H.W., 1976. pKa-Werte von Ethidiumbromid und 7-Amino-391
593 9-phenyl-10- äthyl-phenanthridinium-bromid, Zeitschrift für Naturforschung C 31, 656–
594 660. ISSN (Online) 1865-7125, ISSN (Print) 0939–5075.
595 Zhu, R.L., Chen, Q., Zhou, Q., Xi, Y. Zhu, J., He, H., 2016. Adsorbents based on
596 montmorillonite for contaminant removal from water: A review. Appl. Clay Sci. 123, 239–
597 258.
598

Figure captions

Fig. 1. Uptake of Et^+ on PFL-1 at pH 8. The triangular symbols are the measured values. Solid and dashed lines are the Freundlich and Langmuir fits to the observed data.

Fig. 2. Desorption of metal cations from PFl-1 as affected by the amount of Et^+ adsorption (a), the relationship between cation desorbed, and Br^- and Et^+ adsorbed (b).

Fig. 3. XRD patterns of PFl-1, and PFl-1 with different amounts of Et^+ adsorption from isotherm adsorption (a), and kinetic adsorption (b), at pH 8.

Fig. 4. TG (a) and DTG (b) analyses of raw EtBr, and EtBr adsorbed on PFl-1. The vertical scale of raw EtBr is on the right side; for others it is on the left side.

Fig. 5. SEM image of raw PFl-1 (a), raw EtBr (b), 1.39 CEC PFl-1-EtBr (c), its face scan of Br (red color) and Al (white color) (d), image after heating the 1.39 CEC PFl-1-EtBr sample at 500℃ (e), then face scan of Br (red color) and Al (white color) again (f), their EDS spectra (g), and d-value changes under three temperatures (h~j).

Fig. 6. FTIR spectra of raw PFl-1, crystalline EtBr, and PFl-1 with various EtBr loadings (equivalent to proportion of PFl-1 CEC values) in the wavelength range of 400-4000 cm^{-1} (a), and 400–1800 cm^{-1} (b).

Fig. 7. Illustration of uptake of EtBr on PFl-1 surfaces via the ribbon-like structure under low (left) and high (right) EtBr concentrations.

Title of tables

Table 1. Thermodynamic values of EtBr adsorption on PFl-1 under different temperatures.

Table 2. Band positions of infrared frequencies (cm^{-1}) of EtBr and their corresponding positions after adsorption on PFl-1.

Figures

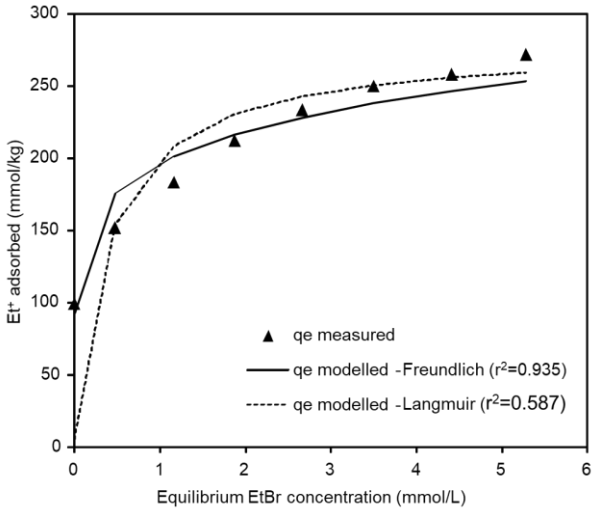

Fig. 1

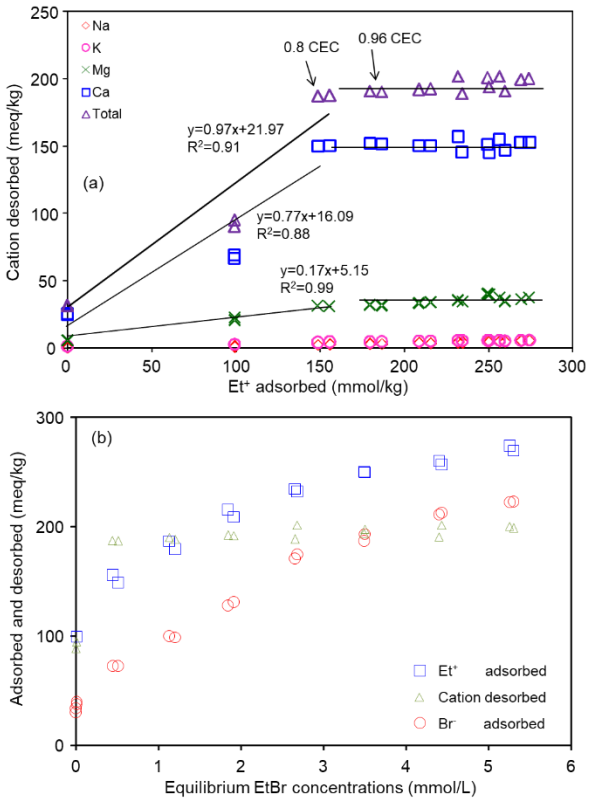

Fig. 2

628

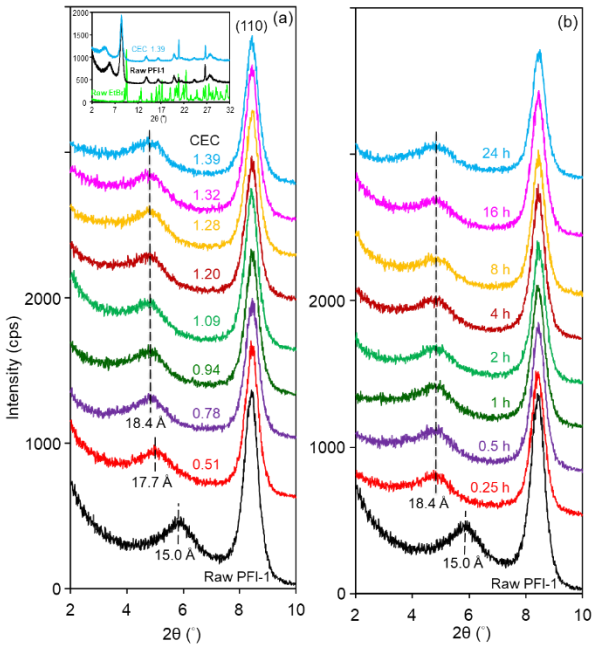

629

630 Fig. 3

631

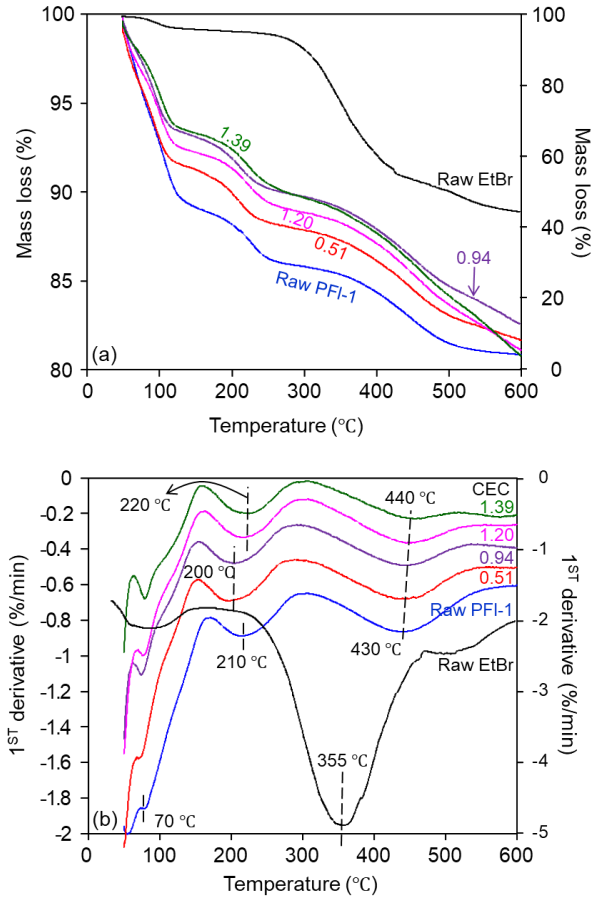
Mass loss (%)
Temperature (℃)
1.39
Raw EtBr
1.20
0.51
0.94
Raw PFI-1
(a)
1ST derivative (%/min)
220 ℃
200 ℃
210 ℃
70 ℃
355 ℃
440 ℃
430 ℃
CEC
1.39
1.20
0.94
0.51
Raw PFI-1
Raw EtBr
(b)

632

633 Fig. 4

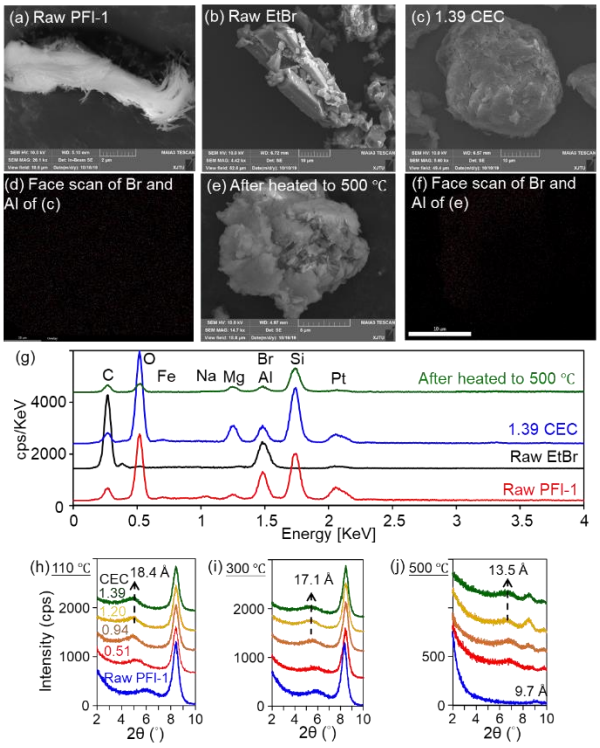

634

635 Fig. 5

636

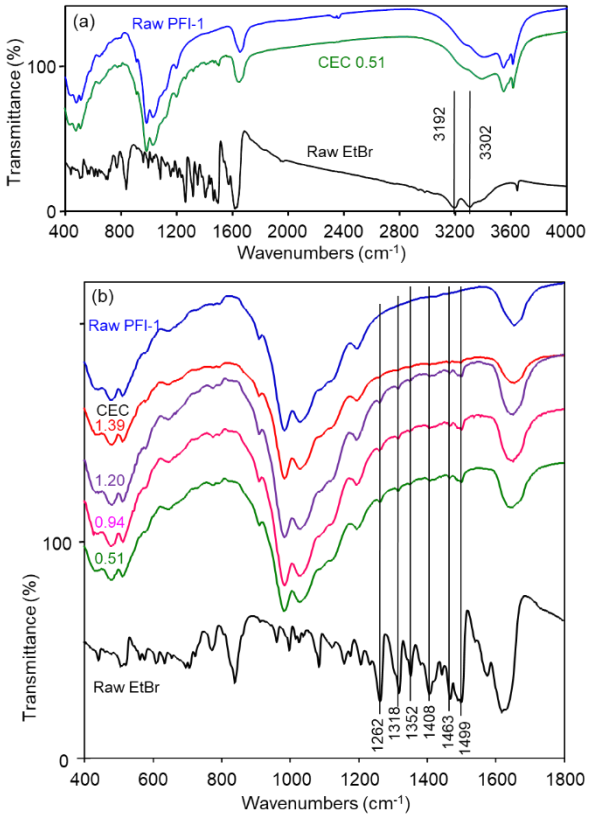

637

638 Fig. 6

639

640

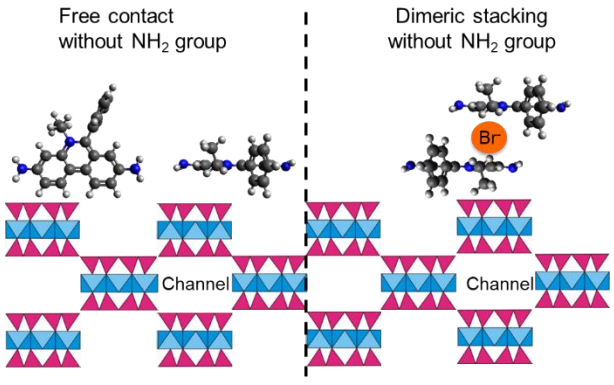

641

642 Fig. 7

643

644 **Tables**

645 Table 1. Thermodynamic values of EtBr adsorption on PFl-1 under different temperatures.

pH	Ln(K_d) (L/Kg)			△G° (kJ/mol)			△H° (kJ/mol)	△S° (kJ/mol K)
	303K	318K	333K	303K	318K	333K		
8	4.73	4.56	4.43	-11.91	-12.09	-12.27	-8.23	0.01

646

647 Table 2. Band positions of infrared frequencies (cm^{-1}) of EtBr and their corresponding positions

648 after adsorption on PFl-1.

EtBr (from reference) [a]	Raw EtBr (this study)	After EtBr adsorption on PFl-1 (this study)	Possible band assignment [a]
3302	3278	3378	ν_s(N–H)
3192	3196	3207	ν_{as}(N–H); ν(C–H); aromatic
1629	1629	1629	δ(N–H)
1578	1568	1578	ν(C=C)(in ring), aromatic
			ν(C=O) + ν(C=N)
			δ(C–H) deformation
			Ring breathing bands
1499	1496	1498	ν(C=N)
1489	1478	1500	ν(C=C)

1408	1404	1406	ν(C–H) δ(C–H)
1352	1350	1350	ν(C–C) + ν_{as}(C–N) C–H rock, alkanes
1319	1317	1317	ν_s(C–N)
1262	1261	1265	δ(C–H) in plane bending
1207	1203	1203	δ_{rock}; NH
837	837	837	C–H out of plane bending
773	771	771	δ_{rock}, C–H rock skeletal vibrations
706	704	704	CNC deformation

[a] (Eldaroti et al., 2013).

Supplementary Information for:

Mechanistic insights into ethidium bromide removal by palygorskite from contaminated water

Po-Hsiang Chang[a,*], Binoy Sarkar[b,*]

[a] *School of Human Settlements and Civil Engineering, Xi'an Jiaotong University, 28 Xianning West Road, Xi'an, Shaanxi, 710049, P.R. China*

[b] *Lancaster Environment Centre, Lancaster University, Lancaster, LA1 4YQ, United Kingdom*

[*] Corresponding author. Email: tectonicion@xjtu.edu.cn (P.-H. Chang); b.sarkar@lancaster.ac.uk (B. Sarkar)

Calculation of EtBr surface coverage

- The SSA of PFl-1 is 136.35 m^2/g = (136.35 x 10^{20}) $Å^2/g$
- The EtBr adsorption capacity is 0.275 mmol/g = (0.275 x 10^{-3}) mol/g
- Area covered by each EtBr molecule = (SSA of PFl-1)/(EtBr adsorption capacity x N)

where, N is the Avogadro's number (6.02 x 10^{23}).

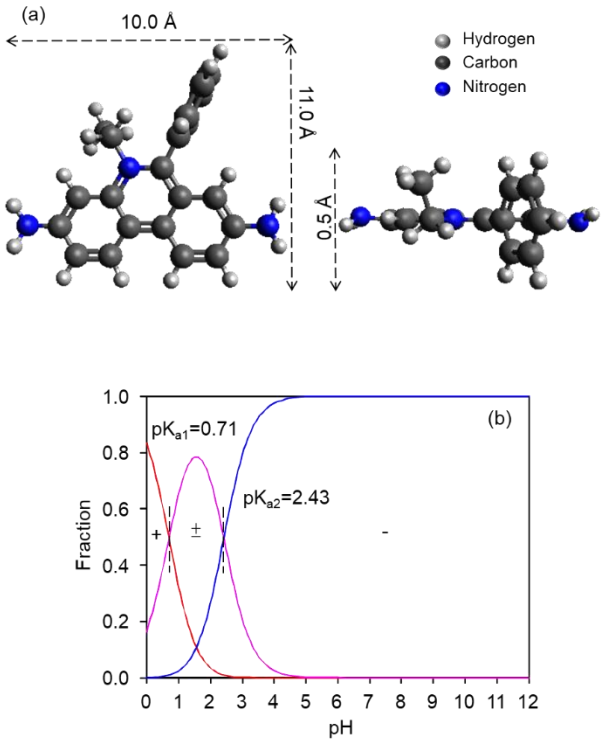

Fig. S1. Molecular structure of EtBr as two view (a), and its speciation under different pH values (b).

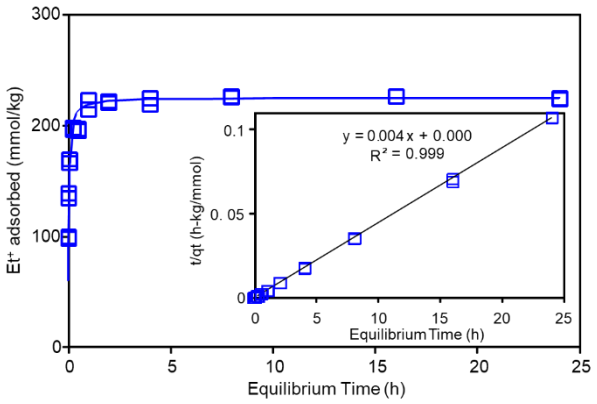

672

673 Fig. S2. Kinetics of Et^+ uptake on PFl-1 at pH 8 under initial EtBr concentration of 4 mmol/L.

674 The solid line is pseudo-second-order fit to the observed data. Inserts is the linear plot of Eq. (1).

675

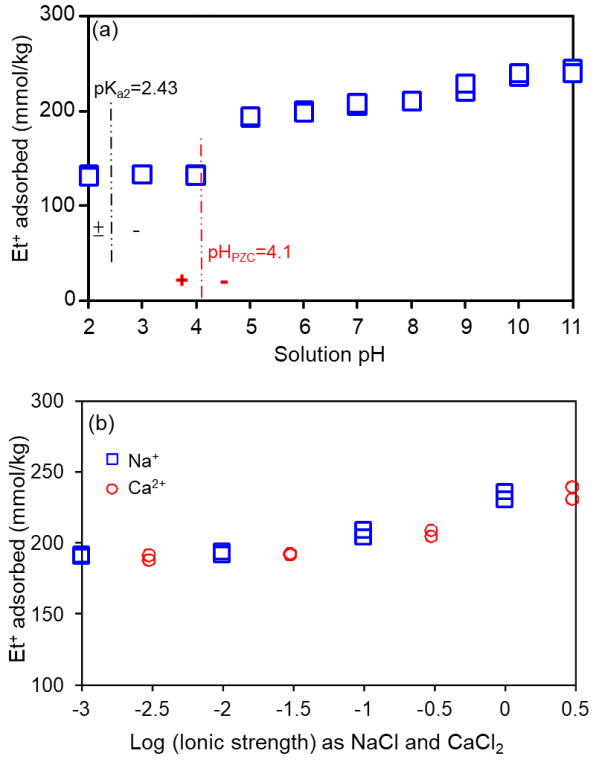

676

677 Fig. S3. Et^+ uptake on PFl-1 as affected by equilibrium solution pH (a), and ionic strengths (b),

678 from an initial EtBr concentration of 4 mmol/L.

679

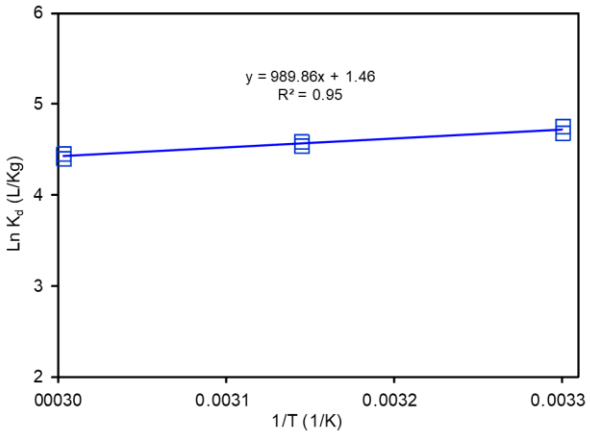

680

681 Fig. S4. Et^{+} adsorption on PFl-1 as affected by equilibrium temperature at pH 8 from an initial

682 EtBr concentration of 4 mmol/L.